Optical implementation of iterative fractional Fourier transform algorithm

Joonku Hahn, Hwi Kim, and Byoungho Lee

School of Electrical Engineering, Seoul National University, Kwanak-Gu Shinlim-Dong, Seoul 151-744, Korea
byoungho@snu.ac.kr

http://oeqelab.snu.ac.kr

Abstract: An optical implementation of iterative fractional Fourier transform algorithm is proposed and demonstrated. In the proposed implementation, the phase-shifting digital holography technique and the phase-type spatial light modulator are adopted for the measurement and the modulation of complex optical fields, respectively. With the devised iterative fractional Fourier transform system, we demonstrate two-dimensional intensity distribution synthesis in the fractional Fourier domain and three-dimensional intensity distribution synthesis simultaneously forming desired intensity distributions at several multi-focal planes.

OCIS codes: (070.2580) Fourier optics; (090.1760) Computer holography; (230.6120) Spatial light modulators.

References and links

1. J. Turunen and F. Wyrowski, *Diffractive Optics for Industrial and Commercial Applications* (John Wiley and Sons Ltd., New York, 1997).
2. B. Kress and P. Meyrueis, *Digital Diffractive Optics: An Introduction to Planar Diffraction Optics and Related Technology* (John Wiley and Sons Ltd., New York, 2000).
3. H. Kim, K. Choi, and B. Lee, "Diffractive optic synthesis and analysis of light fields and recent applications," Jpn. J. Appl. Phys. **45**, 6555-6575 (2006).
4. V. A. Soifer, V. V. Kotlyar, and L. Doskolovich, *Iterative Methods for Diffractive Optical Elements Computation* (Tayor & Francis Ltd., London, 1997).
5. T. Shirai and T. H. Barnes, "Adaptive restoration of a partially coherent blurred image using an all-optical feedback interferometer with a liquid-crystal device," J. Opt. Soc. Am. A **19**, 369-377 (2002).
6. J. Hahn, H. Kim, K. Choi, and B. Lee, "Real-time digital holographic beam-shaping system with a genetic feedback tuning loop," Appl. Opt. **45**, 915-924 (2006).
7. H. Kim and B. Lee, "Optimal nonmonotonic convergence of the iterative Fourier-transform algorithm," Opt. Lett. **30**, 296-298 (2005).
8. H. Kim, B. Yang, and B. Lee, "Iterative Fourier transform algorithm with regularization for the optimal design of diffractive optical elements," J. Opt. Soc. Am. A **12**, 2353-2365 (2004).
9. K. Choi, H. Kim, and B. Lee, "Synthetic phase holograms for auto-stereoscopic image display using a modified IFTA," Opt. Express **12**, 2454-2462 (2004).
10. H. M. Ozaktas and D. Mendlovic, "Fractional Fourier Optics," J. Opt. Soc. Am. A **12**, 743-751 (1995).
11. A. Sahin, H. M. Ozaktas, and D. Mendlovic, "Optical implementation of the two-dimensional fractional Fourier transform with different orders in the two dimensions," Opt. Commun. **120**, 134-138 (1995).
12. A. Sahin, H. M. Ozaktas, and D. Mendlovic, "Optical implementations of two-dimensional fractional Fourier transforms and linear canonical transforms with arbitrary parameters," Appl. Opt. **37**, 2130-2141 (1998).
13. H. M. Ozaktas, M. A. Kutay, and Z. Zalevsky, *The Fractional Fourier Transform with Applications in Optics and Signal Processing* (John Wiley and Sons Ltd., New York, 2001).
14. D. Mendlovic, Y. Bitran, R. G. Dorsch, C. Ferreira, J. Garcia, and H. M. Ozaktaz, "Anamorphic fractional Fourier transform: optical implementation and applications," Appl. Opt. **34**, 7451-7456 (1995).
15. T. Kim and T-C. Poon, " Three-dimensional matching by use of phase-only holographic information and the Wigner distribution," J. Opt. Soc. Am. A **12**, 2520-2528 (2000).
16. P. Andrés, W. D. Furlan, G. Saavedra, and A. W. Lohmann, "Variable fractional Fourier processor: a simple implementation," J. Opt. Soc. Am. A **14**, 853-858 (1997).
17. E. Tajahuerce, G. Saavedra, W. D. Furlan, E. E. Sicre, and P. Andrés, "White-light optical implementation of the fractional Fourier transform with adjustable order control," Appl. Opt. **39**, 238-245 (2000).

#74650 - $15.00 USD Received 5 September 2006; revised 31 October 2006; accepted 31 October 2006

18. I. Yamaguchi and T. Zhang, "Phase-shifting digital holography," Opt. Lett. **22**, 1268-1270 (1997).

1. Introduction

Diffractive optical element (DOE) is one of key elements in the complex optical information processing systems that can be used as phase and amplitude filters mainly for synthesizing desired optical field distribution or compensating wave-front aberrations [1-3]. Hence, one of the important related issues is the optimal design of DOEs. Usually, regarding the optical field synthesis, the pre-requisite computational design based on well-established theoretical models should be prepared ahead [4], and the practical implementation of the optical field synthesis system follows. However in the system which is hard to model numerically or whose numerical parameters change in real time, this process is incomplete in synthesizing desired optical field distribution. For dynamically compensating the aberration of a real system, the adaptive optical methods with feedback functions are required [5, 6]. These adaptive methods solve for the adequate phase profiles compensating the aberration. The more active method of synthesizing desired optical field distribution is the optical implementation of a DOE design algorithm in a real system. This optical implementation has advantages that DOE is designed optimally in the real system which may have a distributed aberration and that the additional feedback function is not demanded.

The most popular algorithm for DOE design is the iterative Fourier transform algorithm (IFTA) [7-9]. When the optical system between a DOE and a specified image plane is represented by the fractional Fourier transform (FRFT) description, the algorithm may be referred to iterative FRFT algorithm. The iterative FRFT algorithm repeats a forward FRFT and an inverse FRFT with constraints on the input and output planes. In Fig. 1, the iterative FRFT algorithm is illustrated. By transforming the optical fields in the input and the output planes iteratively, the DOE profile and the diffraction image are improved gradually. The general iterative FRFT algorithm must be equipped with the proper constraints existing in the input and output planes. The hard constraint in the input plane can take into account the functional relationship between phase and amplitude modulations. The soft constraint produces the degrees of freedom for the optimization of DOE phase profiles, which is significantly influent on the convergence of the iteration. The iterative FRFT has distinctive feature that the inverse transform of the *a*th order FRFT is substituted for its complementary (2-*a*)th order FRFT.

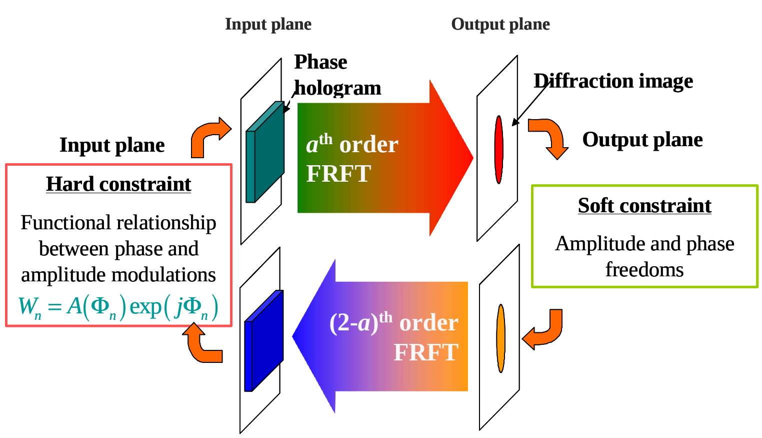

Fig. 1. Iterative FRFT algorithm.

The optical implementation of the iterative FRFT algorithm includes measuring and reconstructing the optical field as well as the optical implementation of a FRFT. The FRFT theory has been actively researched in the optical information processing fields [10-13]. The firmly established operator approach originated from the FRFT theory gives more systematic management and insightful understanding of general complex optical information processing system that the simple use of the generalized Fresnel transform cannot provide [14-17]. The phase-shifting holography technique is the most important dynamic optical field measurement techniques using charge-coupled devices (CCDs) [18]. With the phase-shifting holography technique, the wave-front of diffraction fields generated in optical information processing systems can be accurately measured and additionally the reconstruction of measured optical field is possible using spatial light modulators (SLMs) with the electrical controllability.

In this paper, as a prerequisite step for eventual realization of dynamic and adaptive optical field synthesis, an optical implementation of iterative FRFT algorithm is proposed and the convergence of this algorithm is studied. The *a*th order FRFT and its complementary (2-*a*)th order FRFT are constructed optically. By combining two complementary systems and using the phase-shifting holography technique, the iterative FRFT algorithm is optically realized. The validity and feasibility of the proposed implementation is proven with some related experimental results.

This paper is organized as follows. In Sec. 2, the optical implementation of FRFT is described. In Sec. 3, the optical implementation of iterative FRFT algorithm is proposed. In Sec. 4, experimental results are presented and discussed. In Sec. 5, conclusion and perspective are given.

2. Optical implementation of fractional Fourier transforms

The scheme of the iterative FRFT algorithm is composed of several parts. The forward FRFT and its inverse FRFT are basically necessary. The constraint functions at the input and output planes should also be devised so that they can be optically implemented. In this section, the optical implementation of FRFT is discussed.

At first we should choose an implementation form of FRFT appropriate for our objective. The *a*th order two-dimensional fractional Fourier transform is defined by

$$F_\alpha(u,v)=\int_{-\infty}^{\infty}\int_{-\infty}^{\infty}K_\alpha(u,v,u',v')G(u',v')du'dv', \tag{1}$$

where the integral kernel is defined by,

for $a\neq 2m$, $$K_a(u,v,u',v')=\left[1-j\cot\left(\frac{\pi a}{2}\right)\right]\exp\left(j\pi\left[\cot\left(\frac{\pi a}{2}\right)\left(u^2+v^2\right)-2\csc(\pi a/2)(uu'+vv')+\cot\left(\frac{\pi a}{2}\right)\left(u'^2+v'^2\right)\right]\right), \tag{2a}$$

for $a=4m$, $$K_a(u,v,u',v')=\delta(u-u')\delta(v-v'), \tag{2b}$$

for $a=4m\pm 2$, $$K_a(u,v,u',v')=\delta(u+u')\delta(v+v'), \tag{2c}$$

where m is an integer. The important properties of the fractional Fourier transform are the associative and the communicative properties as

$$F_{a1}\left[F_{a2}(f)\right]=F_{a2}\left[F_{a1}(f)\right]=F_{a1+a2}(f). \tag{2d}$$

In general, paraxial optical system can be described with the well-defined FRFT. The *a*th order two-dimensional FRFT in optical system is defined by the linear integral transform

$$F(x,y)=\int_{-\infty}^{\infty}\int_{-\infty}^{\infty}h(x,y,x',y')G(x',y')dx'dy', \tag{3a}$$

where the transform kernel is given by

$$h(x,y,x',y')=\frac{\csc(a\pi/2)}{s^2M}e^{-j\pi/2}\exp\left(j\frac{\pi\left(x^2+y^2\right)}{\lambda R}\right)\exp\left(\frac{j\pi}{s^2}\left[\cot\left(\frac{\pi a}{2}\right)\frac{\left(x^2+y^2\right)}{M^2}-\frac{2\csc(\pi a/2)}{M}(xx'+yy')+\cot\left(\frac{\pi a}{2}\right)\left(x'^2+y'^2\right)\right]\right). \tag{3b}$$

#74650 - $15.00 USD Received 5 September 2006; revised 31 October 2006; accepted 31 October 2006

The above kernel may be found in Ref. 13, and it maps a function $G(x',y')=(1/s)\hat{G}(x/s,y/s)$ into $[1/(sM)]\exp\left(j\pi\left(x^2+y^2\right)/(\lambda R)\right)\hat{G}_a\left(x/(sM),y/(sM)\right)$, where $\hat{G}_a(u,v)$ is the ath order two-dimensional fractional Fourier transform of $\hat{G}(u,v)$.

Let us consider the optical system shown in Fig. 2. This is an optical implementation of the cascade of the ath order two-dimensional FRFT and its complementary (2-a)th order FRFT. Form Eq. (2d) we see that the overall system is an FRFT with the order of 2 because a+(2-a)=2. Then, from Eq. (2c) we see that this overall system is just inversing the image in transverse coordinates from $G(x_1,y_1)$ to $F(x_3,y_3)$, which should be true because the overall system is a 4-f imaging system. A diverging spherical wave is incident on the filter denoted by $G(x_1,y_1)$ and the optical field on the filter is Fourier-transformed to $P(x_2,y_2)$ that is given by

$$\begin{aligned}P(x_2,y_2)&=\frac{-j}{\lambda f}\int\!\!\int\left[\exp\left(j\pi\frac{\left(x_1^2+y_1^2\right)}{\lambda R}\right)G(x_1,y_1)\right]\exp\left(-j\frac{2\pi}{\lambda f}(x_2x_1+y_2y_1)\right)dx_1dy_1\\&=\frac{-j}{\lambda f}\exp\left(-j\pi\frac{\left(x_2^2+y_2^2\right)}{\lambda R}\right)\int_{-\infty}^{\infty}\int_{-\infty}^{\infty}\exp\left(j\frac{\pi}{\lambda}\left[\frac{\left(x_1^2+y_1^2\right)}{R}-\frac{2}{f}(x_2x_1+y_2y_1)+\frac{\left(x_2^2+y_2^2\right)}{R}\right]\right)G(x_1,y_1)dx_1dy_1,\end{aligned}\tag{4}$$

where, R is the radius of the spherical phase, with which the input optical field $G(x_1,y_1)$ is wrapped.

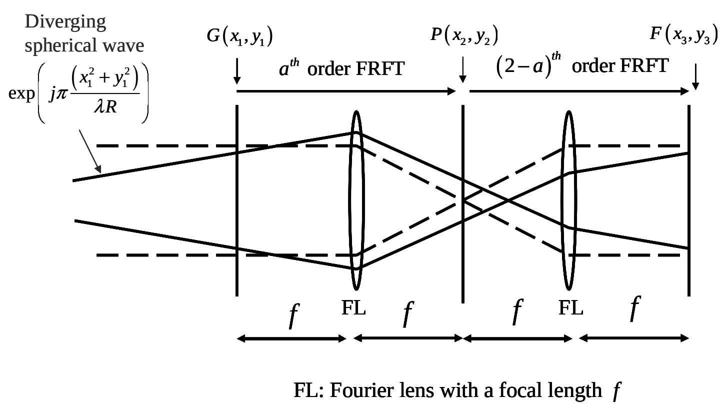

Fig. 2. Optical implementation of the ath order and its complementary (2-a)th order two-dimensional FRFT. The incident optical field may be diverging, converging or normally incident to the input plane.

Since we are of interest in the intensity distribution of the output optical field $P(x_2,y_2)$, the extra quadratic phase term $\exp\left(-j\pi\left(x_2^2+y_2^2\right)/\lambda R\right)$ can be neglected in Eq. (4). Comparing Eqs. (3b) and (4), we can estimate the transform order and the scaling factor of the corresponding FRFT, respectively, as

$$a=\frac{2}{\pi}\arccos\left(\frac{f}{R}\right),\tag{5a}$$

$$s^4=\frac{\lambda^2R^2f^2}{R^2-f^2}.\tag{5b}$$

The second section of the total optical system in Fig. 2 indicated by the (2-a)th order fractional Fourier transform is similarly analyzed. To construct the (2-a)th order fractional Fourier transform, the converging phase factor $\exp\left(j\pi\left(x_2^2+y_2^2\right)/\lambda R'\right)$ must be multiplied by the

#74650 - $15.00 USD Received 5 September 2006; revised 31 October 2006; accepted 31 October 2006

optical field $P(x_2, y_2)$, where $-R'$ is the converging radius of curvature ($R' > 0$). Then the optical field is Fourier-transformed to $F(x_3, y_3)$. The second stage is equivalent to the first stage except the sign change of the incident spherical phase factor. Then the transform order of the second stage can be found just by changing R with $-R'$:

$$2 - a = \frac{2}{\pi}\arccos\left(-\frac{f}{R'}\right), \tag{6a}$$

$$s^4 = \frac{\lambda^2 R^2 f^2}{R^2 - f^2}. \tag{6b}$$

As pointed out earlier, the overall system of Fig. 2 is a 4-*f* imaging system, i.e., the image $F(x_3, y_3)$ is the same as $G(x_1, y_1)$ in Fig. 2 except the coordinate inversion. Hence the (2-*a*)th order FRFT, which is called a complementary transform for the *a*th order FRFT, can be considered as the inverse transform of the *a*th order FRFT. We can control the FRFT order *a* by adjusting the curvature *R* of the incident spherical field as can be seen in Eq. (5a). With changing the sign of the curvature of the incident spherical wave, we can realize the forward FRFT and its inverse FRFT in the same FRFT optic setup. This is an important factor to be made use of to optically implement the iterative FRFT algorithm.

3. Optical implementation of iterative fractional Fourier transform algorithm

In this section, the proposed optical implementation of the iterative FRFT algorithm is elucidated. The functional parts of the implemented system and the algorithmic equipments necessary for the iterative FRFT can be separately explained.

Figure 3 shows the schematic of the implemented system. As indicated in Fig. 3, the system is composed of several functional parts of (a) the field measurement part using the phase shifting holography technique, (b) the 1st beam path with a negative lens for the *a*th order FRFT, (c) the 2nd beam path with a positive lens for the (2-*a*)th order FRFT, (d) the 4-*f* imaging system for matching the scaling factors between the CCD and the SLM, and (e) LabView-based system control unit.

Coherent Verdi 5W Nd:YAG laser with wavelength of 532 nm is used as a light source. The field measurement part is composed of the piezo stage XYZ-38 of Piezosystem Jena and the CCD (KODAK MegaPLUS ES1.0/MV with 8 bit resolution) with the pixel size of $9\mu m$. The optical field distribution is measured by the phase-shifting holography technique.

The 1st and 2nd beam paths share an SLM composed of the liquid crystal device (SONY LCX016AL-6) with the pixel size of $24\mu m$ and two polarizers placed before and after the liquid crystal device. To optimally control the phase modulation of SLM in the full range of 2π, the rotation angles of the former and latter polarizers to the reference axis parallel with the SLM are tuned as 330° at the input side and 10° at the output side, respectively. Mechanical shutters (SIGMA KOKI 65GR) are used to switch the 1st and 2nd beam paths automatically. The 1st beam path and the 2nd beam path are corresponding to the *a*th order FRFT and the (2-*a*)th order FRFT, respectively. In the 1st beam path a negative lens (denoted by NL in Fig. 3) is placed to wrap the phase profile on the SLM with the spherical phase of the radius R, and on the other side, in the second beam path, a positive lens (PL) is placed to provide the spherical phase of the radius $-R'$. A pattern mask describing the target intensity distribution is placed on the 2nd beam path (the inverse transform).

#74650 - $15.00 USD Received 5 September 2006; revised 31 October 2006; accepted 31 October 2006

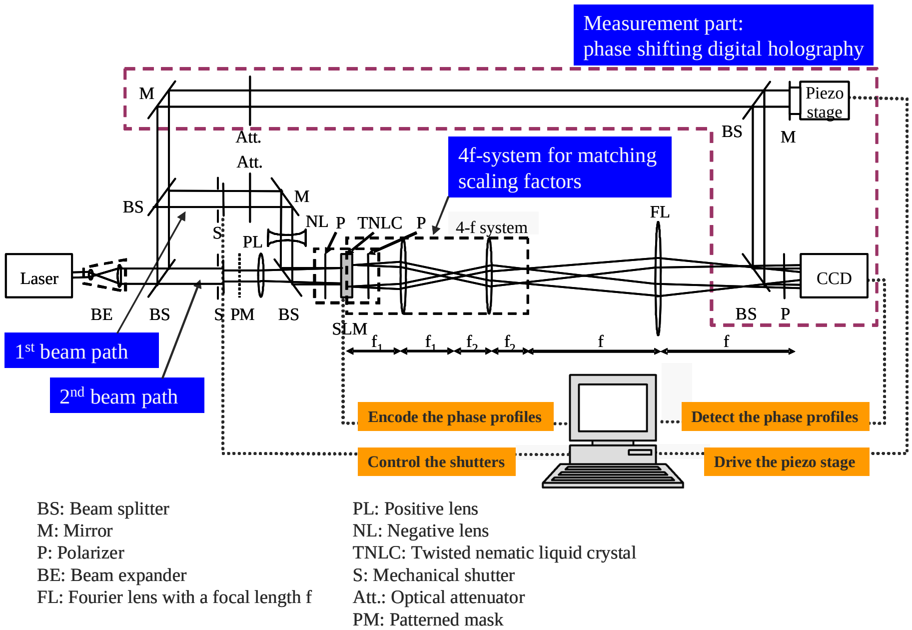

Fig. 3. Optical implementation of the iterative FRFT algorithm.

Especially, the optical field information measured by the CCD is transferred to the SLM after signal processing of the phase-shifting digital holography. Here the scale of the field distribution is magnified because the pixel size of the SLM ($24\mu m$) is bigger than that of CCD ($9\mu m$). However, matching the scaling factors between the CCD and the SLM is necessary to correctly carry out the forward and the inverse FRFTs. The scaling factor mismatch will result in very complicated FRFT relation [5]. To avoid this difficulty, a 4-*f* imaging optic setup with magnification feasibility is employed for matching the scaling factors of the SLM and the CCD. By the 4-*f* imaging optics, the optical field represented on the SLM is adjusted to fit the scale of the CCD.

The iterative FRFT algorithm is composed of several algorithmic parts: (a) the forward FRFT, (b) the inverse FRFT, (c) the hard constraint function in the input plane, and (d) the soft constraint function in the output plane. In addition, (e) the adjustable optics for controlling the spherical curvature of the incident spherical wave is necessary. With these equipments, we can perform the three-dimensional intensity distribution synthesis simultaneously forming desired intensity distributions at several multi-focal FRFT planes as well as two-dimensional intensity distribution synthesis in the fractional Fourier domain. Some experimental results are presented in the next section.

Basically, the algorithmic flow chart of the iterative FRFT algorithm follows that presented in Fig. 1. However, in the optical implementation, additional steps of adding and subtracting spherical phase profile from the measured phase profile have to be inserted at every iteration step as shown in Fig. 4. At the first step, the initial phase profile in the input plane is obtained by the inverse transform from the patterned mask representing the signal domain, where the inverse transform is implemented by the (2-*a*)th order FRFT. At the following steps, the forward and the successive inverse transforms are conducted iteratively. The beam paths are selected by mechanical shutters to implement the *a*th order FRFT (1st beam path) and the (2-*a*)th order FRFT (2nd beam path) alternatively. That is, the *a*th order FRFT and the (2-*a*)th order FRFT in Fig. 1 are split into time sequential steps along the 1st and 2nd beam paths.

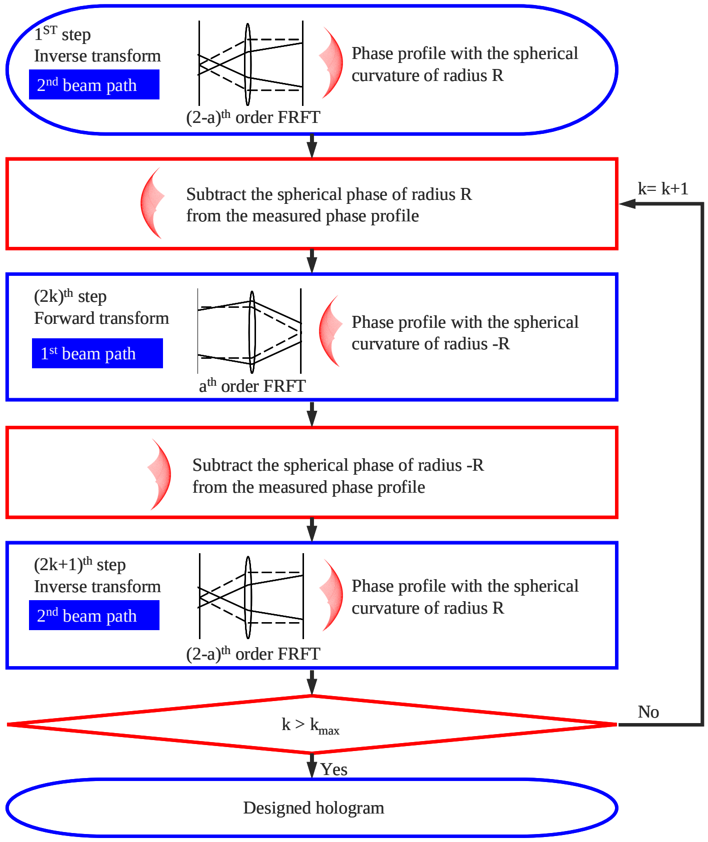

Fig. 4. Flow chart of the iterative FRFT algorithm.

Between the steps the spherical phases are subtracted from the measured phase profiles, and at the following step the conjugate spherical phases are added to the phase profile encoded on the SLM, since the spherical phase with the small radius compared with the pixel size of the encoded phase profile cannot be correctly represented by the SLM. This problem results from a discrete sampling of the spherical phase.

A soft clipping method is devised to realize the soft constraint in the output plane. For this, the inverse transform is conducted twice as shown in Fig. 5. First, the optical field on the signal area selectively filtered by the patterned mask is inversely transformed and next, the optical field on both the signal and noise areas is inversely transformed. Two inversely transformed field distributions are summed with specific weight factors. The ratio of the weight factors is controlled to be decreased as the iteration progresses.

With this system, the DOE phase profile generating a wanted two-dimensional intensity distribution at the *a*th order FRFT domain can be attained through this iteration procedure. With additional control of the spherical curvature of the incident spherical wave, we can obtain different intensity distributions at different FRFT domains. Multiplexing several DOE phase profiles enable simultaneous generation of intensity distributions at several FRFT domains with different FRFT orders. In other words, two-dimensional intensity distribution synthesis in the fractional Fourier domain and three-dimensional intensity distribution synthesis simultaneously forming desired intensity distributions at several multi-focal planes can be realized in real time with the devised iterative FRFT system.

#74650 - $15.00 USD
Received 5 September 2006; revised 31 October 2006; accepted 31 October 2006

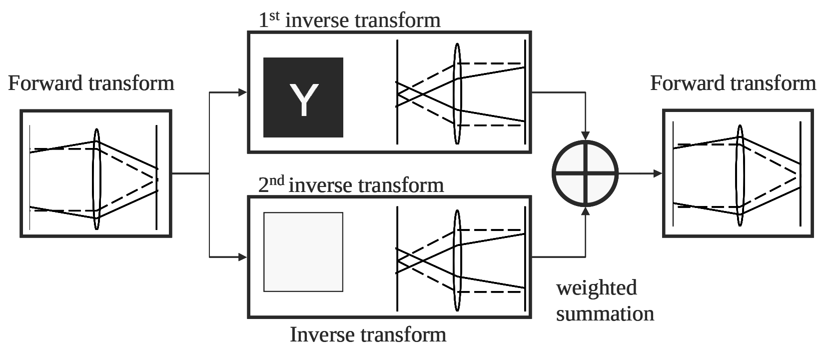

Fig. 5. Soft clipping in the iterative FRFT algorithm.

Regarding the three-dimensional multi-focal intensity distribution synthesis, we can see that when the DOE with the phase profile obtained by the proposed system at the *a*th order FRFT domain is illuminated by a plane wave, the diffraction pattern is formed at the defocused plane. In Fig. 6, the transform of the wave wrapped with diverging spherical phase (denoted by dotted lines) to the focal plane is formulated as

$$P(x_2,y_2)=\frac{-j}{\lambda f}\int_{-\infty}^{\infty}\int_{-\infty}^{\infty}\left[\exp\left(j\pi\frac{\left(x_1^2+y_1^2\right)}{\lambda R}\right)G(x_1,y_1)\right]\exp\left(-j\frac{2\pi}{\lambda f}(x_2x_1+y_2y_1)\right)dx_1dy_1, \tag{7a}$$

and the transform of the plane input wave (denoted by the solid line) modulated by $G(x_1,y_1)$ to a Δd distance from the focal plane is formulated as

$$F(x_2,y_2)=\frac{-j}{\lambda f}\int_{-\infty}^{\infty}\int_{-\infty}^{\infty}\left\{\exp\left[\frac{j\pi}{\lambda f}\left(\frac{-\Delta d}{f}\right)\left(x_1^2+y_1^2\right)\right]G(x_1,y_1)\right\}\exp\left(\frac{-j2\pi}{\lambda f}(x_2x_1+y_2y_1)\right)dx_1dy_1. \tag{7b}$$

By comparing the integrands of Eqs. (7a) and (7b), the relation between the radius R and the defocus Δd is given by

$$\Delta d=-f^2/R\ . \tag{7c}$$

Therefore, with several positive and negative lens pairs of radius R and $-R$, we can design DOE phase profiles to generate diffraction images at distinguished image planes. Also, the obtained DOE phase profiles can be multiplexed to form three-dimensional multi-focal intensity distribution at several distinguished planes.

4. Experimental results

In this section, it is demonstrated with experiments that the DOE phase profile is optically designed by the proposed implementation of the iterative FRFT algorithm. As mentioned in the previous section, the location of the output plane depends on the radius of the spherical phase used in the stage of performing the iterative FRFT algorithm. Figure 7(a) shows the improvement of diffraction images as the iteration progresses with the spherical phase of radius $R=\infty$ (i.e. a plane wave input). Figure 7(b) shows the improvement for the case in which the spherical phase of the radius $R = 62mm$ is used. In both cases, the focal length of the Fourier lens is set to $f = 150mm$. The FRFT order of the first case is 1 and the stagnation of the iteration is reached at the 16th iteration stage, where the ratio in soft clipping is set to zero. The FRFT order of the second case is a complex number 0.9746*j* and the stagnation of the iteration is arrived at the 7th iteration stage, where the ratio in soft clipping is set to zero.

Received 5 September 2006; revised 31 October 2006; accepted 31 October 2006
13 November 2006 / Vol. 14, No. 23 / OPTICS EXPRESS 11110

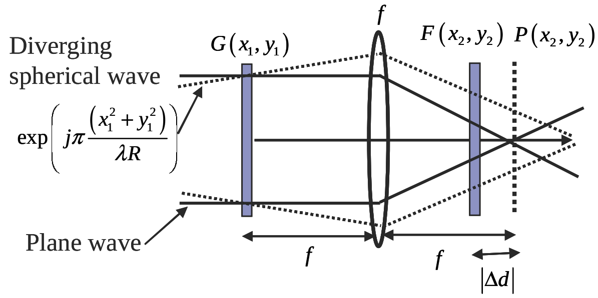

Fig. 6. The relationship for the two transforms: input with the spherical radius R (dotted lines) and the plane wave input with the corresponding defocus Δd .

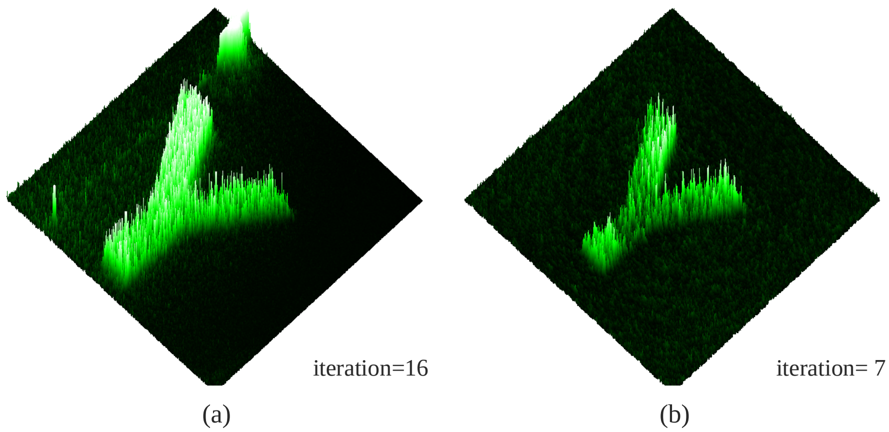

Fig. 7. Improvement of diffraction images as the number of iteration increases in the iterative FRFT algorithm for the two conditions of the radius of the spherical phase: (a) $R=\infty$ (0.24 MB movie) and (b) $R=62mm$ (0.13 MB movie).

In our another experiment, four DOE phase profiles are designed with different patterned masks being applied with different spherical phases as shown in Fig. 8. Based on the principle of Fig. 6, by multiplexing obtained DOE phase profiles, the overall DOE can form desired intensity distributions at several different longitudinal locations simultaneously as shown in Fig. 9. Since the diffraction images are detected after the incident beam passes through the lens, the converging spherical phases are applied to designed DOE phase profiles. In Fig. 9, we see that diffraction images are changed with the change in the image-capturing location of the CCD.

5. Conclusion

With the devised iterative FRFT algorithm, we can design the DOE phase profile to generate two-dimensional intensity distribution in a certain defocused plane at a time without modeling the real system. The proposed technique is implemented in the almost fully optical way and we can simplify the processes such as measuring the real system parameters and encoding the DOE phase profile into the SLM. With the FRFT by an incident spherical phase profile, we show that the FRFT order at the lens focal plane is controllable and the amount of the defocus has a clear relationship with the FRFT order at the lens focal plane. We successfully realized an optical implementation of iterative FRFT algorithm with the aid of wave-optical engineering technologies like the SLM and the phase-shifting digital holography technique.

#74650 - $15.00 USD Received 5 September 2006; revised 31 October 2006; accepted 31 October 2006

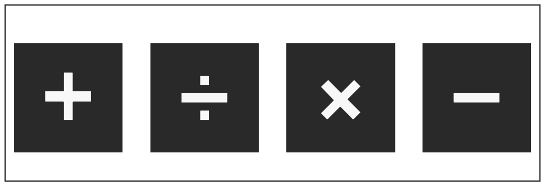

(a)

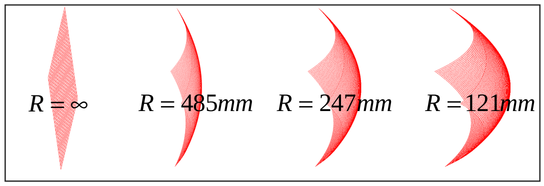

(b)

Fig. 8. Multiplexing four DOE phase profiles (a) the patterned masks and (b) the applied spherical phase profiles.

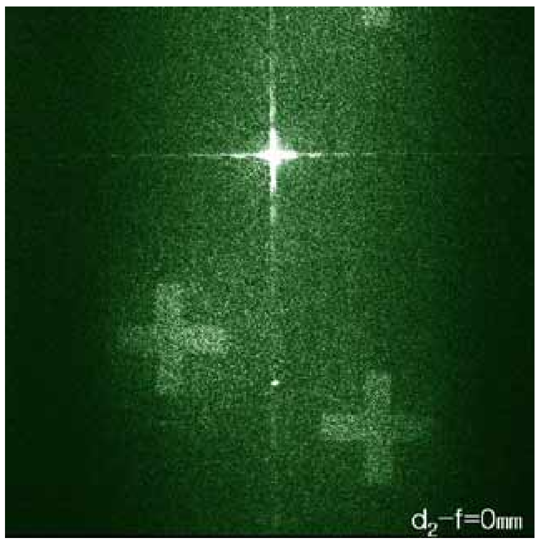

Fig. 9. (0.88 MB movie) Diffraction images of the multiplexed DOE captured by a CCD as the capturing location is changed.

With the FRFT language, the forward and the inverse transform are clearly defined and the optical implementation is also manageable. A noticeable engineering point in this work is the 4-*f* imaging part for matching the scaling factors of the CCD and the SLM. By adjusting the spherical phase curvature, we can obtain the DOE phase profiles to generate diffraction images at several defocused planes. The experimental feasibility of multi-focal image synthesis using the simple DOE multiplexing method opens the possibility of shaping three-dimensional volumetric intensity distribution synthesis in volumetric region by using a fully optical implementation setup.

In short, we studied the optical implementation of an iterative algorithm and the convergence of the algorithm. Based on this work we will improve the adaptive optical field synthesis algorithm compensating the distributed aberration in a real time.

Acknowledgment

This work was supported by Samsung SDI., Ltd.